Journal of Solid State Chemistry 182 (2009) 223–228

Contents lists available at ScienceDirect

Journal of Solid State Chemistry

journal homepage: www.elsevier.com/locate/jssc

Synthesis and photocatalytic performances of $BiVO_4$ by ammonia co-precipitation process

Jianqiang Yu [a,b,*], Yan Zhang [b], Akihiko Kudo [c,d,**]

[a] Laboratory of Fiber Materials and Modern Textile, Institute of Multifunctional Materials, Qingdao University, No. 308 Ningxia Road, Qingdao 266071, China
[b] School of Chemistry, Chemical Engineering and Environment, Qingdao University, No. 308 Ningxia Road, Qingdao 266071, China
[c] Department of Applied Chemistry, Faculty of Science, Tokyo University of Sciences, 1-3 Kagurazaka, Shinjuku-ku, Tokyo 162-8601, Japan
[d] Core Research for Evolutional Science and Technology, Japan Science and Technology Agency (CREST, JST), 4-1-8 Honcho, Kawaguchi-shi, Saitama 332-0012, Japan

ARTICLE INFO

Article history:
Received 29 May 2008
Received in revised form
16 September 2008
Accepted 19 October 2008
Available online 29 October 2008

Keywords:
$BiVO_4$
Visible-light photocatalysis
Methylene blue decomposition
O_2 evolution

ABSTRACT

This paper reports the preparation and photocatalytic performance of Bismuth vanadate ($BiVO_4$) by a facile and inexpensive approach. An amorphous $BiVO_4$ was first prepared by a co-precipitation process from aqueous solutions of $Bi(NO_3)_3$ and NH_4VO_3 using ammonia. Followed by heating treatment at various temperatures, the amorphous phase converted to crystalline $BiVO_4$ with a structure between monoclinic and tetragonal scheelite. The crystallization of $BiVO_4$ occurred at about 523 K, while the nanocrystalline $BiVO_4$ were formed with a heat-treatment of lower than 673 K. However, when the heat-treatment was carried out at 773 K, the accumulation of nanocrystals to bulk particles was observed. The photocatalytic performances of the materials were investigated by O_2 evolution under visible-light, and MB decomposition under solar simulator. The results demonstrated that the crystalline structure is still the vital factor for the activities of both reactions. However, the crystallinity of $BiVO_4$ gives a major influence on the activity of O_2 evolution, whereas the surface area, plays an important role for photocatalytic MB decomposition.

1. Introduction

The photocatalytic splitting of water into hydrogen and oxygen, and the photocatalytic degradation of organic pollutants are promising reactions for solving urgent energy and environmental issues that confront mankind today. Since the photoelectrochemical water splitting (the Honda–Fujishima effect) was reported in 1972, [1] great progresses have been made on the research and application of photocatalysis both in energy and environmental fields. To date, these researches focused mainly on two directions: one of which is to design and develop visible-light-responsive photocatalysts, because the utilization of visible-light, which accounts for more than half of the solar spectrum, is significant. Another direction is to improve the photocatalytic reactivity and efficiency by optimization of experimental conditions, by synthesizing new types of photocatalysts, or by chemical and physical modifications of known photocatalysts.

Bismuth vanadate ($BiVO_4$) belongs to the group of ternary bismuth oxide compound, Bi–M–O (M = Mo, W, V, Nb and Ta), which exhibits unique physical and chemical properties. $BiVO_4$ has been explored as ferroelastic, [2–19] acousto-optical, [3,4] ion conductive [5] and pigmentary [20,21] materials. More interestingly, $BiVO_4$ synthesized by an aqueous process showed excellent photocatalytic O_2 evolution property from an aqueous $AgNO_3$ solution under visible-light irradiation [22–28]. This highly oxidative reactivity of $BiVO_4$ induced by the visible-light irradiation promotes its applications in oxidative decomposition of environmental pollutions. However, up to now the extensive application in environmental remediation is not got along well, because the small surface area of bulk $BiVO_4$ is unfavorable for the adsorption/desorption kinetics of organic pollutants onto the surface of photocatalyst, which affect significantly on their photocatalytic oxidation and decomposition. Therefore, it is necessary to find strategies to improve the visible-light photocatalytic reactivity and efficiency of $BiVO_4$ for organic pollutants decomposition. In this aspect, one effective approach is the preparation of extremely small-sized photocatalyst either by nano-techniques or by dispersing photocatalysts onto a support

* Corresponding author at: School of Chemistry, Chemical Engineering and Environment, Qingdao University, No. 308 Ningxia Road, Qingdao 266071, China. Fax: +86 532 8378 0378.
** Also for correspondence. Department of Applied Chemistry, Faculty of Science, Tokyo University of Sciences, 1-3 Kagurazaka, Shinjuku-ku, Tokyo 162-8601, Japan. Fax: +81 3 5228 8267.
E-mail addresses: jianqyu@qdu.edu.cn (J. Yu), a-kudo@rs.kagu.tus.ac.jp (A. Kudo).

0022-4596/$ - see front matter © 2008 Elsevier Inc. All rights reserved.
doi:10.1016/j.jssc.2008.10.021

(SiO_2, Al_2O_3, zeolites). For example, TiO_2 nano-sized particles of less than 10 nm show significant enhancement in photocatalytic reactivity attributed to the quantum-size effect, [29–33] due to the electronic state variation of TiO_2 as well as to the short distance required for the photogenerated electron–hole pairs to reach the surface. Another effective approach is the direct synthesis of microporous or mesoporous photocatalysts. This approach may provide the photocatalyst a large surface area, which is favorable for kinetic adsorption/desorption of organic pollutants, and therefore enhance the photocatalytic reactivity and efficiency [34].

For $BiVO_4$, many advance approaches, including solid-state or melting reaction, [35–37] aqueous, [22–26,38] sol–gel, [39–44] and hydrothermal processes, [27,28,45–48] had been developed to prepare $BiVO_4$. Each of these approaches led to a characteristic crystalline structure, which thus showed significant differences in the photocatalytic performances. We have found previously that an amorphous $BiVO_4$ may be synthesized by ammonia co-precipitation method [28]. This method is a facile and inexpensive process, and may be adopted to disperse $BiVO_4$ onto a support, or to form a porous $BiVO_4$. In this paper, we first report the photocatalytic performances of the crystalline $BiVO_4$ samples prepared by calcinations of the amorphous precursor at various temperatures. The structure and crystallization of the prepared samples were characterized by several physico-chemical techniques in order to make a full understand for the materials.

2. Experimental section

2.1. Preparations

Twelve millimole of ammonium metavanadate (NH_4VO_3, Kanto Chemical, purity: 99.5%) and 12.0 mmol of $Bi(NO_3)_3 \cdot 5H_2O$ were dissolved separately into 50 ml of 2.0 mol L^{-1} nitric acid solution, then mix them together to obtain a stable and yellow homogeneous solution. Increase the pH of the above mix solution by dropwise titration of ammonia solution (Kanto Chemical, 28–30% NH_3) under stirring, orange precipitates were obtained. Followed by adjusting the pH to 9 for an entire precipitation, the orange slurry was filtered and dry (denoted as $BiVO_4$(a) in the text). The dried samples were heated at 473, 523, 573, 673 and 773 K (denoted as $BiVO_4$(a)-473, $BiVO_4$(a)-523, $BiVO_4$(a)-573, $BiVO_4$(a)-673, and $BiVO_4$(a)-773, respectively) on atmospheric pressure.

For the purpose of comparison, bulk $BiVO_4$ was also prepared by a solid-state reaction following [36]. Stoichiometric amounts of $Bi(NO_3)_3 \cdot 5H_2O$ and NH_4VO_3 were mixed in a mortar. The mixture was then heated in an oven at 393 K for 24 h to remove crystal water. The mixture was ground again in a mortar and calcined at 973 K for 8 h (denoted as BiVO4(s)).

2.2. Characterization

X-ray powder diffraction (XRD) patterns were measured using an X-ray diffractometer (Rigaku; MiniFlex) with Cu $K\alpha$ radiation ($\lambda = 0.1541$ nm). The crystallite size was estimated using the Scherrer formula:

$$D = K\lambda/(\sqrt{\beta_s^2 - \beta_e^2}\cos\theta$$

where D is the crystalline size, λ is the wavelength of the X-ray radiation (0.1541 nm), K usually taken as 0.89, β_s, β_e are the peak widths at half-maximum height of sample and the equipment broadening, respectively, $2\theta = 34.6^\circ$. Field-emission scanning electron microscope (FE-SEM) images were obtained by electron microscope (JEOL JSM-6700F). The thermogravimetry (TG) and differential thermal analysis (DTA) were performed using a TG–DTA instrument (ULVAC TGA9600) under air flow of 100 mL min^{-1} with a heat rate of 10 K min^{-1} from room temperature to 1073 K. Diffuse reflection spectra were obtained using a UV–Vis–NIR spectrometer (JASCO: Ubest V-570) and were converted from reflection to absorption by the Kubelka–Munk method. Raman spectra were recorded using a Raman spectrometer (JASCO NRS-3200). A red-laser (785 nm) was used as the excitation source.

2.3. Photocatalysis

The photocatalytic decomposition of methylene blue (MB) and the photocatalytic O_2 evolution from an aqueous silver nitrate solution were used as model reactions to determine the photocatalytic properties of the synthesized materials. The photocatalytic O_2 evolution reaction was carried out in a closed gas circulation system. A total content of 0.2 g of the catalyst power was dispersed by a magnetic stirrer in an aqueous $AgNO_3$ solution (0.05 mol/L, 150 mL) in a reaction cell made of Pyrex glass. The light source was an ozone-free 300-W Xe-illuminator (Ushio-CERMAX, LX300). A cutoff filter (Kenko, L-42 ($\lambda > 420$ nm)) was employed for visible-light irradiation. The amount of O_2 evolved was determined by a gas chromatography (Shimadzu GC-8A, TCD, Ar carrier).

The photocatalytic decomposition of MB was carried out in a glass reactor. A total content of 0.2 g of the powdered photocatalyst was suspended in a solution of MB (40 μmol L^{-1}, 50 mL), which was prepared by dissolving the MB powder in distilled water in a Pyrex glass cell at room temperature. A solar simulator (Yamashita YSS-80QA, 200 W Xenon arc lamp) was used as the optical system. The amount of MB decomposition was determined by UV/Vis spectroscopy (JASCO Ubest V-570).

3. Results and discussions

3.1. The crystalline structure of $BiVO_4$

Fig. 1 shows the X-ray diffraction patterns of samples prepared by ammonia co-precipitation. The patterns of the solid-state prepared sample ($BiVO_4$(s)) and zircon-structure ($BiVO_4$(z)) were also included for comparison. The sample prepared by solid-state reaction at 973 K for 8 h ($BiVO_4$(s)) showed a pure phase monoclinic scheelite $BiVO_4$. For the synthesized samples, the diffraction peaks that index zircon-type $BiVO_4$ were not observed clearly, instead, all the peaks match well to the monoclinic scheelite $BiVO_4$. This result suggests that the synthesized materials by ammonia co-precipitation are of characteristic scheelite $BiVO_4$. However, these samples are not well-distorted monoclinic scheelite $BiVO_4$.

As we have known, $BiVO_4$ has three main crystal forms: zircon-structure with tetragonal system and scheelite structure with monoclinic and tetragonal systems. The crystal structure of monoclinic scheelite $BiVO_4$ is much similar to that of tetragonal scheelite, except for the distortion. The Bi–O polyhedron in the former is more distorted than that of tetragonal scheelite $BiVO_4$ due to the presence of a $6s^2$ lone pair of Bi^{3+}. In XRD patterns, these distinctive differences are reflected by that monoclinic scheelite $BiVO_4$ generally shows a peak at 15° and well splitting of peaks at 18.5°, 35°, and 46° of 2θ. It is, therefore, convenient to distinguish monoclinic and tetragonal scheelite $BiVO_4$ from XRD patterns. It is observed from the crystalline $BiVO_4$ synthesized by ammonia co-precipitation method that no peak at 15° of 2θ can be observed, and the peaks at 18.5°, 35°, and 46° of 2θ are not well splitted. These observations suggested that the structures of the

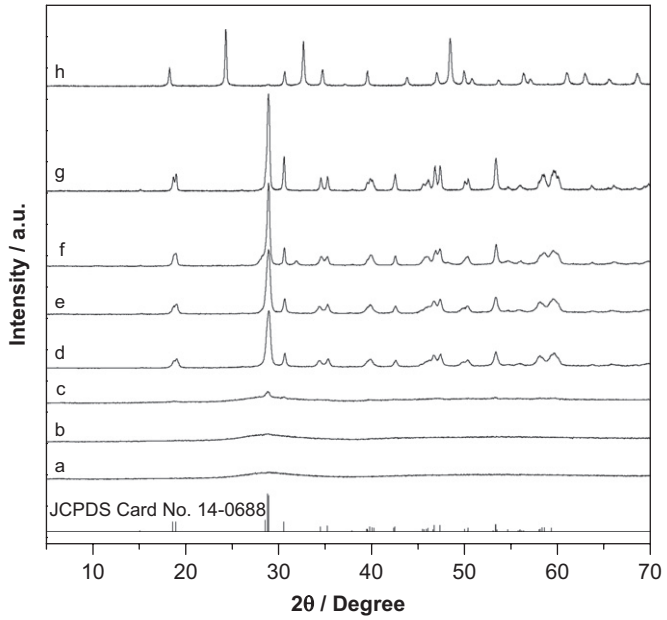

Fig. 1. X-ray diffraction patterns of (a) $BiVO_4$(a), (b) $BiVO_4$(a)-473, (c) $BiVO_4$(a)-523, (d) $BiVO_4$(a)-573, (e) $BiVO_4$(a)-673, (f) $BiVO_4$(a)-773, (g) $BiVO_4$(s), and (h) $BiVO_4$(z).

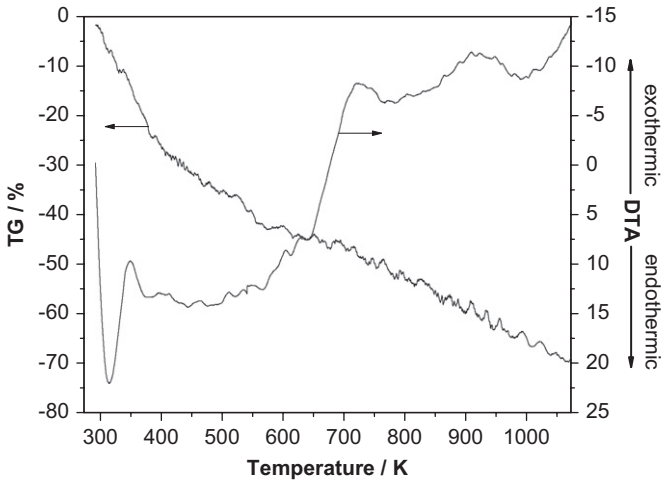

Fig. 2. TG–DTA curves of the amorphous $BiVO_4$(a) prepared by co-precipitation of $Bi(NO_3)_3$ and NH_4VO_3 solution using aqueous ammonia.

coprecipitated samples are of monoclinic scheelite type, but with less distortion.

3.2. *Effect of heat-treatment on the crystallization of $BiVO_4$*

Fig. 2 shows the TG and DTA curves of amorphous $BiVO_4$(a) prepared by a co-precipitation process using aqueous ammonia. Three steps of weight loss in the TG curve, and one endothermic together with two exothermic peaks in the DTA curve were observed. The endothermic peak, which corresponding to the first step of weight loss in TG curve below 378 K, is attributed to the evaporation of adsorbed water. The second step of weight loss from 378 K to about 573 K, which has no corresponding thermal peak, is attributed to the elimination of surface hydroxyl groups and the remains of ammonium or nitrate ions. The first exothermic peak observed from 483 to 653 K, corresponding to the weight loss of about 10%, was attributed to the crystallization of $BiVO_4$ into scheelite phase. However, the phase transition between monoclinic scheelite and tetragonal scheelite structure of $BiVO_4$ reversibly occurs at about 528 K. The second much large exothermic peak from 653 to 773 K may be due to the sintering of small particulars into large particles. The continuous weight loss from 773 to 1073 K, which corresponds to a large amount of heat emit, is suspected to be associated with the reformation of $BiVO_4$ or the phase transformation at high temperature [49].

The crystallization process of $BiVO_4$ dependent upon heat-treatment temperature can be determined clearly by the X-ray diffraction patterns (Fig. 1). $BiVO_4$(a) shows an amorphous phase, judging from the broad peak at about 29° in the XRD pattern. The crystallization of $BiVO_4$(a) was not observed until the heat-treatment temperature increased to 523 K, in which the broad peak at about 29° in XRD pattern begins to sharpen. Upon the heat-treatment temperature increased to higher than 573 K, the formation of crystalline $BiVO_4$ was observed. As the temperature was improved from 573 to 773 K, an increase in the diffraction peaks intensities of $BiVO_4$ was observed, indicative of well-crystallized $BiVO_4$ were gradually formatted. However, the half-width of the (1 0 1) peak is getting narrow, suggesting that the sizes of the crystallites grow with increasing the temperature. When the temperature was further improved to 773 K, an impurity peak at 32° (Fig. 1 f, the asterisk) was observed, indicating that high temperature is not beneficial for a pure phase $BiVO_4$ formation. This structure was directly crystallized from the amorphous phase even at the temperature as low as 523 K.

The above results suggested that the crystallization of $BiVO_4$ synthesized by this NH_3 co-precipitation process differs from the reported precipitation method reported by Rustioni [50] and Higgins [51]. They observed that the zircon-structured $BiVO_4$ was first precipitated from a mixed aqueous solution of a bismuth (III) salt and a vanadate salt, while a further treatment, such as aging or crystallization in an aqueous phase or calcination at various temperatures, is then necessary in order to obtain monoclinic scheelite $BiVO_4$. This conclusion seems reasonable, because the phase transition of zircon-type $BiVO_4$ to monoclinic scheelite occurred irreversibly at about 670–770 K, and low temperature is beneficial for the formation of zircon-type $BiVO_4$ [2,6].

Fig. 3 shows the scanning electron microscopy photographs of the $BiVO_4$ powders synthesized by co-precipitation of aqueous ammonia solution, followed by heat-treatment at various temperatures. Lots of tiny size particles were observed for $BiVO_4$(a) (Fig. 2a), suggesting that this sample is a typical amorphous material, in agreement with the XRD pattern (Fig. 1). The samples of $BiVO_4$(a)-473 and $BiVO_4$(a)-523, which were formed by the calcinations of $BiVO_4$(a) at 473 and 523 K, respectively, showed different particle shapes with $BiVO_4$(a). Some particulates accumulate together to form a larger one. The $BiVO_4$(a)-523 appears similar to $BiVO_4$(a)-473, except that some crystal-like particles can be observed in the former micrograph. These crystal-like particles indicated weak diffraction peaks in XRD pattern (Fig. 1c). Therefore, heating BiVO4(a) at a relatively low temperature of 473 K leads to some merging of smaller particles to form larger ones. Upon heating the sample of $BiVO_4$(a) at 573 K for 5 h, solid balls with particle size of estimating to be 50 nm were clearly observed. Higher temperature of 673 K was imposed upon $BiVO_4$(a), the particle size of $BiVO_4$(a)-673 became larger than that of $BiVO_4$(a)-573, but it is still smaller than 100 nm, in the range of nanoscale. A further improvement of the temperature to 773 K, the aggregation of $BiVO_4$ into larger particles occurred. The particle size of $BiVO_4$(a)-773 appears to be about 200 nm.

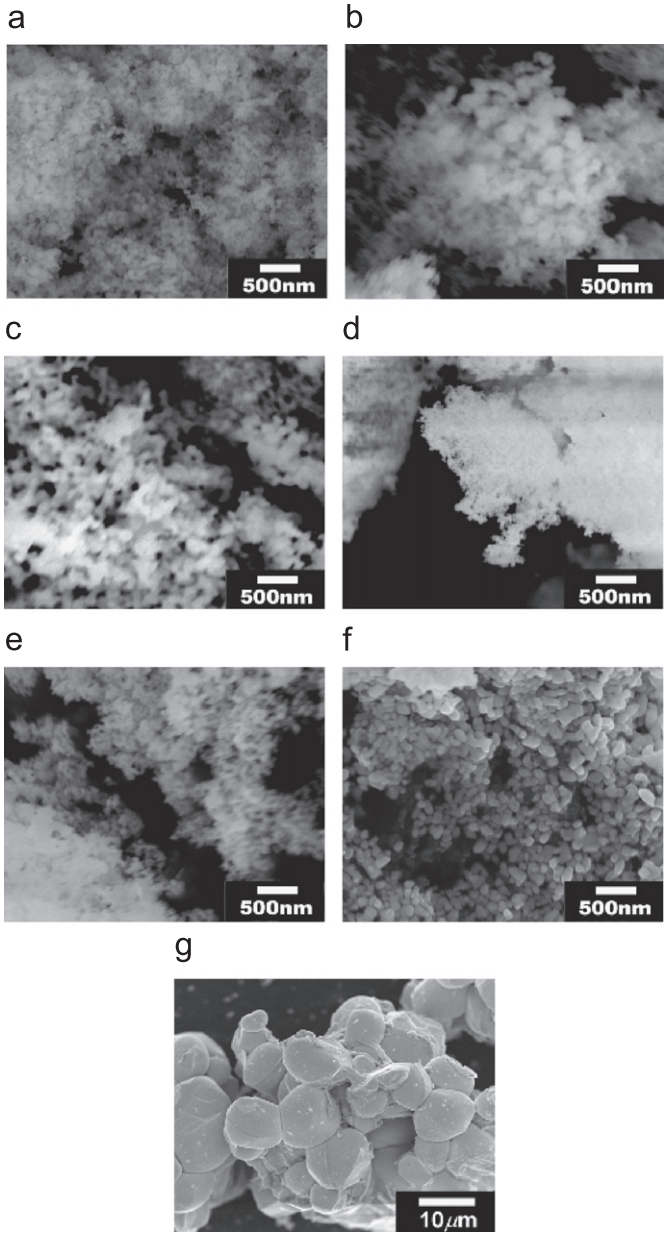

Fig. 3. Typical FE-SEM images of (a) $BiVO_4$(a), (b) $BiVO_4$(a)-473, (c) $BiVO_4$(a)-523, (d) $BiVO_4$(a)-573, (e) $BiVO_4$(a)-673, (f) $BiVO_4$(a)-773, and (g) $BiVO_4$(s).

The formatted $BiVO_4$ has a small crystalline particle size can also be indicated by the width of XRD peaks. From Fig. 1, broadening of diffraction peaks for the synthesized crystalline $BiVO_4$ by ammonia precipitation with comparison to those of $BiVO_4$(s) was observed. Using the Scherrer equation, it is estimated that the primary particle size was 18, 32 and 91 nm for $BiVO_4$(a)-573, $BiVO_4$(a)-673, and $BiVO_4$(a)-773, respectively (Table 1). The surface area of $BiVO_4$(a) is 36 $cm^2 g^{-1}$, 20 times larger that that of $BiVO_4$(s). With the increasing of heat-treatment temperatures, the surface areas of $BiVO_4$ reduce a little.

3.3. The local structure and photophysical property of $BiVO_4$

Raman spectroscopy may provide structural information and is also a sensitive method for the investigation of the crystallization, local structure, and electronic properties of materials. Fig. 4 shows

Table 1
The physical properties of $BiVO_4$ samples by heat-treatment at various temperatures.

Sample	Crystalline size /nm	Surface area /m^2/g
$BiVO_4$(s)	>100 nm	1.8
$BiVO_4$(a)	–	36
$BiVO_4$(a)-473	–	31
$BiVO_4$(a)-523	–	29
$BiVO_4$(a)-573	18	26
$BiVO_4$(a)-673	32	4.2
$BiVO_4$(a)-773	91	7.8

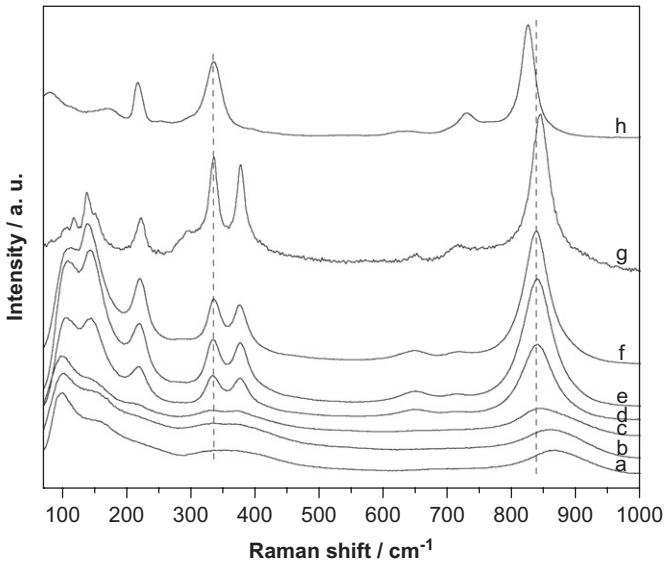

Fig. 4. Raman spectra of (a) $BiVO_4$(a), (b) $BiVO_4$(a)-473, (c) $BiVO_4$(a)-523, (d) $BiVO_4$(a)-573, (e) $BiVO_4$(a)-673, (f) $BiVO_4$(a)-773, (g) $BiVO_4$(s) and (h) $BiVO_4$(z).

the Raman spectra of $BiVO_4$ prepared by ammonium co-precipitation followed by heat-treatment at various temperatures (a–f), and the sample prepared by solid-state reaction (g). The main Raman bands of $BiVO_4$ are observed around 152, 220, 330, 373, 711, and 832 cm^{-1} et al. These bands are the typical vibrational bands of $BiVO_4$ [27,30,31,33,38]. The bands at 152, 220 cm^{-1} are the external vibrations. For comparison the intensity of Raman band, we set the peak at 100 cm^{-1} at a similar level and used as an internal standard.

It was first observed that the intensities of all the vibrational peaks in $BiVO_4$(a), $BiVO_4$(a)-473 and $BiVO_4$(a)-523 are weak, indicating that the amorphous phase cannot gave a resolve Raman band. However, the wavelength of Raman vibrations suggests that all the amorphous substances are $BiVO_4$ but not other material. The Raman bands around 711 and 832 cm^{-1} were attributed to the stretching modes of two different types of V–O bond, and the bands at 330 and 373 cm^{-1} were assigned to asymmetric and symmetric deformation modes of VO_4^{3-} tetrahedron, respectively. The resolving and intensities of the two Raman bands at 330 and 373 cm^{-1} were different from sample to sample. The two Raman vibration bands of $BiVO_4$(a), $BiVO_4$(a)-473, $BiVO_4$(a)-523, and $BiVO_4$(a)-573 merged to a dome. It suggested that the deformation of VO_4^{3-} vibration in the local structure is not strong due to the weak formation of VO_4^{3-} tetrahedral in the amorphous samples.

The stretching vibrational bands at 832 cm^{-1} provided more interesting information on the structural variations. The stretching modes of one shorter V–O bond around 832 cm^{-1} for

crystalline $BiVO_4$ samples ($BiVO_4$(a)-473, $BiVO_4$(a)-523 and $BiVO_4$(a)-573) shifted to low frequency in comparison with that for $BiVO_4$(s). Moreover, with the crystallinity improving by the calcination temperatures increasing, the vibration Raman band of V–O shifted gradually to low frequency. It has been established a functional relationship between the Raman stretching frequencies and the metal-oxygen bond length in the local structure, in which the lower frequency of stretching vibrational Raman band corresponds to the longer bond length [31,52]. So the V–O bond in $BiVO_4$(g) is shorter that that of other crystalline $BiVO_4$ ($BiVO_4$(a)-573, $BiVO_4$(a)-673 and $BiVO_4$(a)-773).

The photophysical properties of $BiVO_4$ powders calcined at various temperatures were detected by diffuse reflectance spectra (DRS). The spectra are shown in Fig. 5. Significant differences in the absorption edge between the amorphous phase ($BiVO_4$(a), $BiVO_4$(a)-473 and $BiVO_4$(a)-523) and the crystalline samples ($BiVO_4$(a)-573, $BiVO_4$(a)-673, and $BiVO_4$(a)-773) are observed. The slope in the absorption edge for the amorphous phases is less steep than those of crystalline samples. As we have known, the absorption edge of $BiVO_4$ was formed by the charge-transfer of the hybrid orbitals of Bi_{6s} and O_{2p} to V_{3d} orbitals. The low slope in the absorption edge of amorphous samples might be attributed to the band-structure were not well formed due to the low crystallinity.

Moreover, the absorption edge of the crystalline samples (profile d, e, f) are blue-shift with comparison to that of $BiVO_4$(s). The absorption edge of a DR spectrum reflects the energy difference between the top of the valence band and the bottom of the conduction band. That is to say, the band gap of a semiconductor can be calculated from the absorption edge. As we have known the band gap of tetragonal scheelite $BiVO_4$ is slightly wider than that of monoclinic scheelite $BiVO_4$, if the ratio of monoclinic scheelite phase to tetragonal scheelite $BiVO_4$ in a sample is low, the band gap will be broader (blue-shift). So, the observed blue-shift in DR spectra might be explained by the low gradient of monoclinic phase. This analysis agrees with the observation of XRD, in which the two peaks around 18.5° are not well resolved.

3.6. The photocatalytic performances

Fig. 6 shows the photocatalytic performances for O_2 evolution from an aqueous $AgNO_3$ solution under visible-light irradiation ($\lambda \geqslant 420$ nm) over the co-precipitation series of $BiVO_4$ together with $BiVO_4$(s) prepared by a solid-state reaction. The $BiVO_4$(a)-673, with an O_2 evolution rate of 26 μmol/h exhibited the highest activity among these samples. $BiVO_4$(a) gave the lowest activity of 0.9 μmol/h, which was much lower than those over crystalline $BiVO_4$ as usual. The activities of $BiVO_4$(s) is 5.9 μmol/h, much lower than that of $BiVO_4$(a)-573, although the local distortion of $BiVO_4$(s) is higher than that of $BiVO_4$(a)-573. The activity of $BiVO_4$(a)-773 is a little lower than that of $BiVO_4$(a)-673 due to the accumulation of nanocrystalline particle to bulk in the former sample. These results demonstrated that the crystallinity and the nanostructure of $BiVO_4$ samples play the major roles to determine the photocatalytic activity of O_2 evolution.

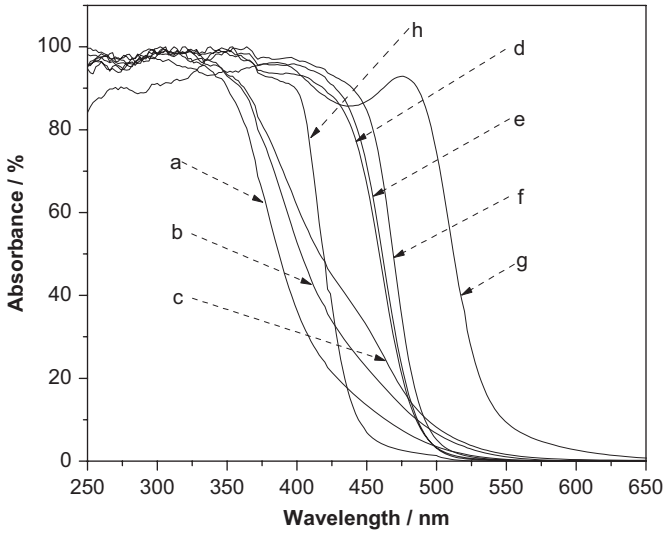

Fig. 5. Diffuse-reflectance spectra of (a) $BiVO_4$(a), (b) $BiVO_4$(a)-473, (c) $BiVO_4$(a)-523, (d) $BiVO_4$(a)-573, (e) $BiVO_4$(a)-673, (f) $BiVO_4$(a)-773, and (g) $BiVO_4$(s).

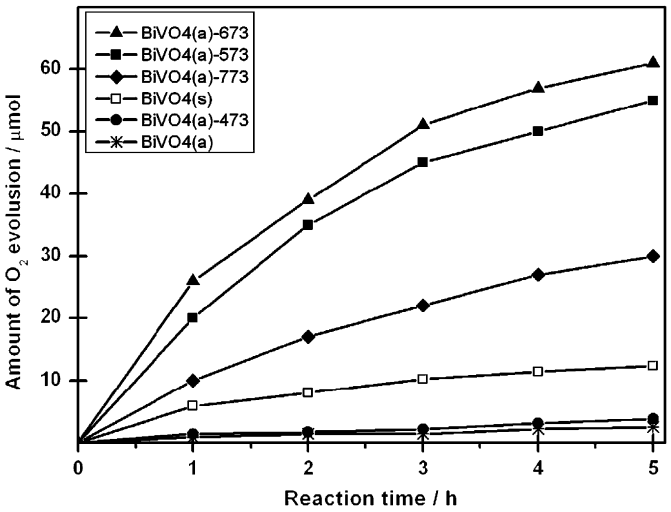

Fig. 6. Photocatalytic O_2 evolution from an aqueous $AgNO_3$ solution (0.05 mol L^1, 150 mL) under visible light irradiation ($\lambda \geqslant 420$ nm) over (a) $BiVO_4$(a), (b) $BiVO_4$(a)-473, (c) $BiVO_4$(a)-523, (d) $BiVO_4$(a)-573, (e) $BiVO_4$(a)-673, (f) $BiVO_4$(a)-773, and (g) $BiVO_4$(s). Reaction conditions: Catalyst: 0.2 g, light source: 300 W Xe lamp attached with a cut-off filter ($\lambda \geqslant 420$ nm). 0.05 mol L^{-1} $AgNO_3$ solution.

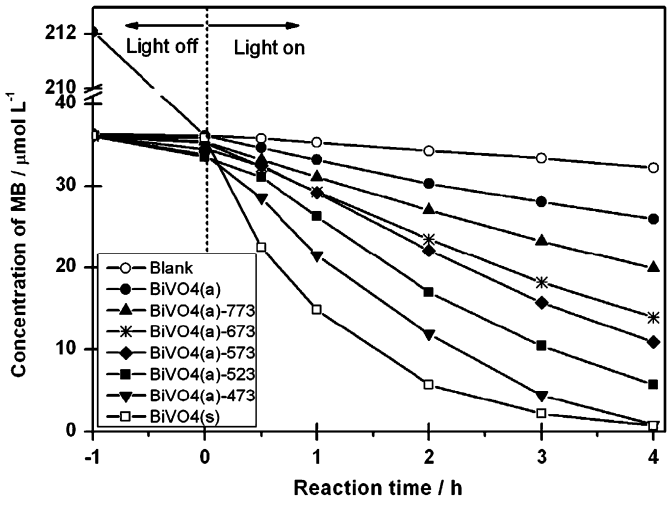

Fig. 7. Photocatalytic decomposition properties of MB under the irradiation of solar simulator over (a) $BiVO_4$(a), (b) $BiVO_4$(a)-473, (c) $BiVO_4$(a)-523, (d) $BiVO_4$(a)-573, (e) $BiVO_4$(a)-673, (f) $BiVO_4$(a)-773, and (g) $BiVO_4$(s). Reaction conditions: Catalyst: 0.2 g, light source: solar simulator (Yamashita Denso, YSS-80QA).

The dependences of MB concentration decreasing with irradiation time over $BiVO_4$ samples under the irradiation of solar simulator are shown in Fig. 7 and Table 2. Without catalyst, the ratio of MB due to photodecomposition after 3 h irradiation was less than 25%. In the presence of $BiVO_4$ photocatalyst, high

Table 2
The photocatalytic activities for methylene blue decomposion under the irradiation of solar simulator.

Sample (0.2 g)	Adsorption under dark /%	Photocatalytic conversion	
		0.5 h/%	4 h/%
Blank	0.65	1.0	23.1
$BiVO_4$(s)	9.54	37.3	96.7
$BiVO_4$(a)	83.0	4.2	28.2
$BiVO_4$(a)-473	6.3	17.0	97.6
$BiVO_4$(a)-523	7.1	7.3	83.0
$BiVO_4$(a)-573	4.4	5.7	68.4
$BiVO_4$(a)-673	2.3	8.3	60.5
$BiVO_4$(a)-773	1.9	6.2	43.7

photocatalytic activity for the decomposition of MB dyes was observed. Because the solution was not recovered to blue as the addition of $AgNO_3$ into the system, indicating that the MB was mineralized by the $BiVO_4$ photocatalyst but not reduced to leuco-MB, which can be reversibly oxidized to MB by $AgNO_3$ [53]. The amorphous $BiVO_4$(a) possessed a much high adsorption ability (83.0%), but gave a low activity for photodecomposition of MB. However, the decomposition ratio of MB increases and reaches the maximum value of nearly 100% when this amorphous $BiVO_4$ was calcined at 473 K for 5 h. Interestingly, $BiVO_4$(a)-473 was still amorphous, and the surface area was large. This observation might be explained that the surface properties of $BiVO_4$ photocatalyst provide a significant effect on the decomposition activity of MB. Because the photobleaching of MB followed the pseudo-first-order kinetics with respect to MB concentration, so the photocatalytic reaction rate depends on the adsorption/desorption property of MB onto the catalysts surface. It is thus reasonable that $BiVO_4$(a)-473 give a high activity, because it possessed a high surface area. As the surface areas reducing with an increasing heat-treatment temperature from 523 to 773 K, the activities were also decreased in this order. The photodecomposition amount of MB over $BiVO_4$(a)-773 was only 43.7%, which was a little higher than that of $BiVO_4$(a). So, the surface area plays an important role on the activity of photocatalytic MB decomposition. It is worthy to note that $BiVO_4$ powder obtained by solid-state reaction showed the highest initial photodecomposition activity among all the samples. It is because that, on the one hand, more component of monoclinic scheelite $BiVO_4$ are present in this sample, judging from the well splitting of peaks at 19° and 35°. On the other hand, the crystallinity of $BiVO_4$(s), which is still the most vital factor that affecting the activity of MB photodecomposition, is higher than that of other samples.

4. Conclusion

A simple method to synthesize nanocrystalline $BiVO_4$ has been established. By adding aqueous ammonium solution into the mix solution of $Bi(NO_3)_3$ and NH_4VO_3 in HNO_3 under room temperature, an amorphous $BiVO_4$ was first formed. By heat-treatment of the amorphous $BiVO_4$ at various temperatures, $BiVO_4$ with the grain size from nanoparticles to bulk materials can be formed. All the crystalline samples were monoclinic scheelite phase. For photocatalytic O_2 evolution reaction, the crystallinity of $BiVO_4$ is a vital factor to affect the reactivity. On the contrary, the surface area instead of the crystallinity is a key factor for the photodecomposition of MB. For both reactions, the $BiVO_4$ synthesized by this approach showed higher efficiency and reactivity than bulk sample.

Acknowledgment

This research was supported by CREST/JST and a Grant-in-Aid (No. 14050090) for the Priority Area Research (No. 417) from MEXT, Japan, and Nissan Science Foundation.

References

[1] A. Fujishima, K. Honda, Nature 238 (1972) 37.
[2] A.R. Lim, S.H. Choh, M.S. Jang, J. Phys.: Condens. Matter 7 (1995) 7309–7323.
[3] C. Manolikas, S. Amelinckx, Phys. Status Solidi A 60 (1980) 167.
[4] S.V. Akimov, I.E. Mnushkina, E.F. Dudnik, Sov. Phys. Technol. Phys. 27 (1982) 500.
[5] K. Hirota, G. Komatsu, M. Yamashita, H. Takemura, O. Yamaguchi, Mater. Res. Bull. 27 (1992) 823–830.
[6] J.D. Bierlein, A.W. Sleight, Solid State Commun. 16 (1975) 69–70.
[7] A. Pinczuk, B. Welber, F.H. Dacol, Solid State Commun. 29 (1979) 515–518.
[8] W.I.F. David, A.M. Glazer, Phase Trans. 1 (1979) 155–170.
[9] C. Manolikas, S. Amelinckx, Phys. Status Solidi A 60 (1980) 167.
[10] A.K. Bhattacharya, K.K. Mallick, A. Hartridge, Mater. Lett. 30 (1997) 7–13.
[11] J.W.E. Mariathasan, R.M. Hazen, L.W. Finger, Phase Trans. 6 (1986) 165–174.
[12] A.R. Lim, S.H. Choh, M.S. Jang, Ferroelectrics 94 (1989) 389–394.
[13] A.R. Lim, J.-H. Chang, S.H. Choh, Phys. Status Solidi B 196 (1996) 33–37.
[14] T.H. Yeom, S.H. Choh, M.L. Du, J. Phys.: Condens. Matter 5 (1993) 2017–2024.
[15] T.H. Yeom, C. Rudowicz, S.H. Choh, Ferroelectrics 156 (1994) 249–254.
[16] T.H. Yeom, S.H. Choh, M.L. Du, M.S. Jang, Phys. Rev. B 53 (1996) 3415–3421.
[17] T.H. Yeom, C. Rudowicz, S.H. Choh, D.G. Mcgavin, Phys. Status Solidi B 198 (1996) 839–851.
[18] P.P. Man, S.H. Choh, J. Fraissard, Solid State Nucl. Magn. Reson. 3 (1994) 231–236.
[19] S.H.Z. Choh, Natureforsch 51a (1996) 591–602.
[20] D. H. Piltingsrud, US Patent 4115141, 1978.
[21] R. W. Hess, US Patent 4115142, 1978.
[22] A. Kudo, K. Omori, H. Kato, J. Am. Chem. Soc. 121 (1999) 11459.
[23] S. Kohtani, S. Makino, A. Kudo, K. Tokumura, Y. Ishigaki, T. Matsunaga, O. Nikaido, K. Hayakawa, R. Nakagaki, Chem. Lett. 31 (2002) 660.
[24] S. Kohtani, M. Koshiko, A. Kudo, K. Tokumura, Y. Ishigaki, A. Toriba, K. Hayakawa, R. Nakagaki, Appl. Catal. B 46 (2003) 573.
[25] S. Kohtani, N. Yamamoto, K. Kitajima, A. Kudo, H. Kato, K. Tokumura, K. Hayakawa, R. Nakagaki, Photoelectrochem. Photobiol. Environ. Energy Fuel (2004) 173.
[26] S. Kohtani, J. Hiro, N. Yamamoto, A. Kudo, K. Tokumura, R. Nakagaki, Catal. Commun. 6 (2005) 185.
[27] J. Yu, A. Kudo, Chem. Lett. 34 (2005) 850.
[28] J. Yu, A. Kudo, Adv. Funct. Mater. 16 (2006) 2163.
[29] M. Anpo, T. Shima, S. Kodama, Y. Kubokawa, J. Phys. Chem. 91 (1987) 4305.
[30] M. Anpo, Y. Kubokawa, Rev. Chem. Intermed. 8 (1987) 105.
[31] M. Anpo, H. Nakaya, S. Kodama, Y. Kubokawa, K. Domen, T. Onishi, J. Phys. Chem. 90 (1988) 1633.
[32] M. Anpo, T. Kawamura, S. Kodama, K. Maruya, T. Onishi, J. Phys. Chem. 92 (1988) 438.
[33] M. Anpo, T. Shima, M. Che, Chem. Express 3 (1988) 403.
[34] G. Li, D. Zhang, J.C. Yu, Chem. Mater. 20 (2008) 3983.
[35] R.S. Roth, J.L. Waring, Am. Mineral. 48 (1963) 1348.
[36] A.W. Sleight, H.-y. Chen, A. Ferretti, Mater. Res. Bull. 14 (1979) 1571.
[37] M. Gotic, S. Music, M. Ivanda, M. Soufek, S. Popovic, J. Mol. Struct. 744 (2005) 535.
[38] S. Tokunaga, H. Kato, A. Kudo, Chem. Mater. 13 (2001) 4624.
[39] A. Galembeck, O.L. Alves, Thin Solid Films 365 (2000) 90.
[40] M.C. Neves, T. Trindade, Thin Solid Films 406 (2002) 93.
[41] K. Hirota, G. Komatsu, M. Yamashita, H. Takemura, O. Yamaguchi, Mater. Res. Bull. 27 (1992) 823.
[42] K. Sayama, A. Nomura, Z. Zou, R. Abe, Y. Abe, H. Arakawa, Chem. Commun. (2003) 2908.
[43] H. Liu, R. Nakamura, Y. Nakato, J. Electrochem. Soc. 152 (2005) G856.
[44] X. Chen, Z. Zhang, Soon W. Lee, J. Solid State Chem. 181 (2008) 166.
[45] J. Liu, H. Wang, S. Wang, H. Yan, Mater. Sci. Eng. B 104 (2003) 36.
[46] B. Xie, H. Zhang, P. Cai, R. Qiu, Y. Xiong, Chemosphere 63 (2006) 956–963.
[47] X. Zhang, Z. Ai, F. Jia, L. Zhang, X. Fan, Z. Zou, Mater. Chem. Phys. 103 (2007) 162–167.
[48] M.T. Weller, Inorganic Materials Chemistry, Oxford University Press, Oxford, UK, 1994.
[49] N. Syam Prasad, K.B.R. Varma, J. Mater. Chem. 11 (2001) 1912.
[50] M. Rustioni, L. Balducci, S. P. A. Montedison, US Patent 4 316 746, 1982.
[51] J. F. Higgins, US Patent 4 063 956, 1977.
[52] D.H. Franklin, I.E. Wachs, J. Phys. Chem. 95 (1991) 5031.
[53] B. Muktha, T. Aarthi, G. Madras, T.N.G. Row, J. Phys. Chem. B 110 (2006) 10280.